Jan Regtmeier[1]
Sebastian Grauwin[1]
Ralf Eichhorn[2]
Peter Reimann[2]
Dario Anselmetti[1]
Alexandra Ros[1]

[1]Experimental Biophysics and Applied Nanoscience, Physics Department, Bielefeld University, Bielefeld, Germany
[2]Condensed Matter Theory, Physics Department, Bielefeld University, Bielefeld, Germany

Original Paper

Acceleration of absolute negative mobility

Recently, the counter intuitive migration phenomenon of absolute negative mobility (ANM) has been demonstrated to occur for colloidal particles in a suitably arranged post array within a microfluidic device [1]. This effect is based on the interplay of Brownian motion, nonlinear dynamics induced through microstructuring, and nonequilibrium driving, and results in a particle movement opposite to an applied static force. Simultaneously, the migration of a different particle species along the direction of the static force is possible [19], thus providing a new tool for particle sorting in microfluidic device format. The so far demonstrated maximum velocities for micrometer-sized spheres are slow, *i.e.*, in the order of 10 nm *per* second. Here, we investigate numerically, how maximum ANM velocities can be significantly accelerated by a careful adjustment of the post size and shape. Based on this numerical analysis, a post design is developed and tested in a microfluidic device made of PDMS. The experiment reveals an order of magnitude increase in velocity.

Keywords: Absolute negative mobility / Microfluidics / Separation

Received: December 23, 2006; revised: March 22, 2007; accepted: March 23, 2007

DOI 10.1002/jssc.200600546

1 Introduction

Channelling and exploiting the unavoidable thermal fluctuations for separation purposes have inspired researchers to study and develop new migration mechanisms, often combined with an application to bioanalytically motivated separation problems. Such novel concepts utilize, *e.g.*, ratchet or steric effects in structured micro- and nanofluidic devices, commonly referred to as lab-on-a-chip systems. Ratchet effects have been proven to generate directed transport of particles [2 – 6] and biomolecules such as DNA [7] and phospholipids [8]. On this basis, an efficient separation method has been developed in a microfluidic device, in which long DNA molecules are separated by continuously streaming through an asymmetric obstacle array [9, 10]. Furthermore, entropic effects have been used to separate long DNA molecules [11], and recently protein separation in similarly designed nanofluidic devices has been reported [12].

A different migration phenomenon, termed absolute negative mobility (ANM), has been observed recently with colloidal particles in a structured microfluidic device [1]. ANM is the motion of objects opposed to a static force and is based on exploiting the interplay of Brownian motion (thermal noise), nonlinear dynamics, and conditions far from thermal equilibrium. All these three ingredients are indispensable for the occurrence of ANM [13, 14]. The applicability of this migration phenomenon for separation purposes has been demonstrated by Regtmeier *et al.* [19] by simultaneously steering two differently sized but like charged particle species into opposite directions.

To understand this migration phenomenon in more detail, the concept of ANM for colloidal particles in a microfluidic device [1, 19] is briefly reviewed here: a linear microfluidic channel has a central area composed of a microstructured post array (see Fig. 1) and two reservoirs at its ends. They are used for supplying buffer and beads and provide the electrical contact *via* immersed electrodes. The necessary conditions, far from thermal equilibrium, are generated by applying an unbiased square wave voltage of amplitude U_0 and period 2τ to the channel, in which noninteracting charged beads (colloidal particles) are randomly distributed after hydrodynamic injection. The beads respond to the square-wave driving voltage with a periodic back and forth motion in x-direction. By convention, a positive voltage induces a force on the particle along the positive x-direction, and *vice versa* for negative voltages. The microstructure, necessary for the nonlinear dynamics, is designed such that posts alternately generate small and large gaps in x- and y-direction (see Fig. 1). The small gaps act as geometric traps, as the constriction is smaller than the diameter of the beads.

Correspondence: Dr. Alexandra Ros, Experimental Biophysics and Applied Nanoscience, Physics Department, Bielefeld University, Universitätsstr. 25, 33615 Bielefeld, Germany
E-mail: alexandra.ros@physik.uni-bielefeld.de
Fax: +49-521-106-2959

Abbreviation: ANM, absolute negative mobility

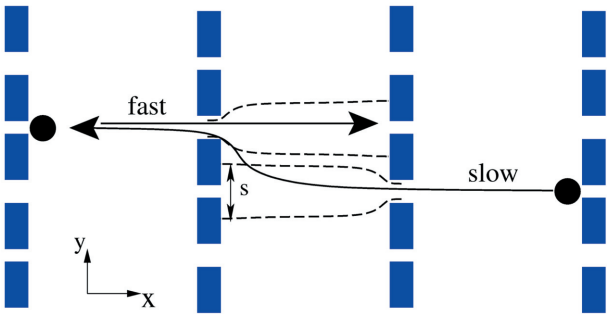

Figure 1. A schematic drawing of a part of the microstructure: The dashed lines indicate the boundaries of the basin of attraction, which a bead has to leave by diffusion in order to avoid a trap. The width of the basin is given by the distance *s*. In the slow direction ($U_{dc} - U_0 < 0$), the bead has more time to diffuse during the migration and thus has a higher probability of avoiding a trap. In the fast direction ($U_{dc} + U_0 > 0$) the migration time is shorter, *i.e.*, the particle remains with a high probability within the basin of attraction and cannot avoid a trap.

Due to the symmetry of the microstructure and the driving signal, no average particle velocity can be observed. However, when an additional static voltage U_{dc} is applied, the migration behavior changes (to be specific, we assume $0 < U_{dc} < U_0$): Let's consider a particle that starts from a trap, when the driving voltage switches to $-U_0$, such that the total voltage results in $U_{dc} - U_0 < 0$. During its migration in the negative *x*-direction the particle has, after passing the large gap midway, a certain probability to cross the boundary of the basin of attraction of the trap ahead (Fig. 1; dashed lines) by diffusion in lateral *y*-direction [15]. To avoid a trap, the distance covered by diffusion must be larger than 1/2 *s*. During the subsequent half-period of duration τ, where $U_{dc} + U_0 > 0$, the total voltage and hence the forces are larger in modulus and of opposite sign. Accordingly, the migration time from one row of posts to the next is shorter and the diffusive dispersion narrower. Likewise, the probability of avoiding a trap is smaller and so is the average traveling distance in the positive *x*-direction. The overall result is a net motion in the negative *x*-direction, *i.e.*, opposite to the positive static DC voltage U_{dc}.

The so far observed maximum ANM velocities were typically in the range of 10 – 20 nm/s [1, 19]. The reason of this slow average migration can be found in a small diffusive dispersion leading to very small probabilities of avoiding a trap. Therefore, the first obvious way to accelerate ANM is to use smaller objects. However, this would be associated with an adaptation of the driving parameters and the size of the microstructure. This approach is not the focus of the present work, but is discussed in some detail in Section 4. The second alternative is to decrease the lateral size of the attraction basin of the traps (denoted by *s* in Fig. 1) by an optimization of the geometry. Thus, the objective of the present paper is to demonstrate an acceleration of ANM for micrometer-sized colloidal particles in solution by changing the size and shape of the posts. With numerical simulations, different alternatives are tested and an optimized geometry is finally set up and used to experimentally demonstrate an acceleration of ANM by approximately one order of magnitude.

2 Materials and methods

2.1 Chemicals and reagents

Disodium hydrogenphosphate dihydrate was obtained from Fluka (Germany). Tween-20 was purchased from Sigma (Germany). The triblock copolymer Pluronic F-108 was a generous gift from BASF (Germany). For all solutions, deionized water from a Milli-Q biocel (Millipore, USA) was used. PDMS (Sylgard 184) was obtained from Spoerle Electronic (Germany), glass microscope slides from Menzel (Germany).

2.2 PDMS devices

A soft lithography process is used to build the microfluidic device: first, a master wafer with the inverted relief of the microstructure was fabricated *via* spincoating a photoresist (SU-8) onto a Si-wafer, UV-exposing through a chromium mask, and development in a developer bath [16]. For UV-exposure, a home-built lithography contact unit was used to ensure a close contact of the mask and the photoresist. Second, the polymer Sylgard 184 was mixed with its curing agent in a 10:1 ratio and poured over the master wafer. After curing for 4 h at 85°C, the crosslinked polymer was peeled off the wafer and the reservoir holes were punched. Before assembly, the microstructured PDMS slab and a PDMS-coated glass slide were oxidized in a home-built oxygen plasma chamber for 30 s. The microfluidic channels were coated with the triblock copolymer F-108 (500 µM in 100 mM phosphate buffer, pH = 8.3) for 18 h, significantly reducing adsorption of colloidal particles [17]. Shortly before the measurements, the coating solution was replaced by a phosphate solution (100 mM, pH 8.3 and 200 µM Tween-20).

2.3 Microparticles

Carboxyl modified polystyrene particles (CML microbeads) of 2.9 µm diameter were purchased from Interfacial Dynamics Corporation (USA). They were characterized regarding the electrokinetic mobility and the diffusion coefficient by video microscopy and subsequent particle tracking. The mobility was obtained as 0.2 $\mu m^2/Vs$ with a deviation of 50% from chip-to-chip, probably because of the different surface properties generating

the different EOF velocities. The diffusion coefficient was determined as $(0.82 \pm 0.07)\,10^{-13}$ m^2/s.

2.4 Detection

Particle movement was recorded on an inverted microscope (Axiovert200, Zeiss, Germany) equipped with bright field and fluorescence detection as well as with an automized x/y-stage (99S008, Ludl Electronic Products, USA) using a $\times 20$ objective (LD Achro Plan $20\times$/0.40 korr, Zeiss, Germany) and a sensitive CCD-camera (Sensicam, LaVision, Germany). The velocity of the colloidal particles was analyzed by particle image velocimetry (PIV) using ImageJ freeware and Plugin MTrack2 (Nico Stuurman, University of California, San Francisco).

2.5 Chip operations

Initial filling of the microchannel was performed by capillary action and application of vacuum to a reservoir. Before the measurement, a PMMA block with reservoir holes and integrated Pt electrodes was pressed onto the PDMS chip and adhered, thus increasing the reservoir size and holding the electrodes in defined places. The square wave voltage with amplitude U_0 and a static offset U_{dc} was applied using two power supplies from FUG (Model MCN 14-2000 and MCN 140-1250, Germany) and a relay circuit. Instrumental control and data acquisition were performed *via* software programmed in LabView (National Instruments, USA).

2.6 Simulation

The electric potential within the structured microchannel was calculated by solving the Laplace equation with mixed boundary conditions. The posts are considered as perfect insulators, whereas the buffer is a perfect conductor, *i.e.*, the electric field lines cannot enter the posts (von Neumann boundary conditions). From the calculated potential, the electric field was derived. By this procedure, the force field can be calculated up to an unknown gauge factor. Based on this field, the motion of a bead in the *x-y* plane of the microstructure was modeled by 2-D stochastic overdamped dynamics of a point-like particle with the posts being represented as hard-wall obstacles (taking into account the finite radius of the particles). The motion in the *z*-direction (channel height) was not simulated, since it decouples in good approximation from the 2-D motion in the *x-y* plane. The unknown gauge factor was determined by reproducing the measured mobility of the particles in the simulation [1, 19]. In this way, the combined effect of the electrophoretic and electroosmotic mobility contributions was captured quantitatively in the simulations [1, 19]. Similarly, the experimentally determined diffusion coefficient was used to quantify the diffusion of the stochastic Langevin dynamics.

3 Results and discussion

Recently, we could experimentally provide the first proof-of-principle of ANM with colloidal particles in solution [1] as well as the possibility to fractionize particles by ANM [19]. The latter is based on the fact that, by a suitable choice of the driving parameters, differently sized but like charged particles can be steered simultaneously into opposite directions. However, the maximum velocities of ANM were in the range of 20 nm/s.

We recapitulated the main principles of ANM in Section 1 and identified the avoidance of particle traps by diffusion as the basic mechanism for the ANM behavior and also the limiting factor causing the small ANM velocities. Therefore, we will focus below on the processes which lead to a more efficient trap avoidance.

The probability of avoiding a trap is determined by the width of the basin of attraction [15] and the time a bead can diffuse in lateral direction during its motion from one row of posts to the next (see Fig. 1). Given fixed driving parameters this probability can be enhanced by, first, a reduction of the diffusion distance necessary to leave the basin of attraction and, second, by guaranteeing that once a bead escapes from the attraction basin, the probability of diffusing back is small.

The first point can be achieved by decreasing the width of the posts in *y*-direction. A closer analysis shows, however, that size reduction is limited: if the posts become too small, pathways along the electric field lines arise that lead to deterministic meandering through the post array, completely destroying the basic ANM mechanism. A similar effect was found in a ratchet array by Huang *et al.* [18] and identified to be responsible for the prevention of ratcheting of small molecules.

The second point is based on the observation that most of the particles diffusively leave the attraction basin of the trap only shortly before they hit one of the posts adjacent to the gap (*i.e.*, close to the points where the dashed lines in Fig. 1 end at the posts). Therefore, if in this region the motion toward the large gap is favored by suitably shaping the posts, a diffusion back into the basin is unlikely, and ANM can be enhanced.

With respect to these considerations, we propose two concepts for the acceleration of ANM: the first consists in reducing the post width, the second in changing the post shape. Table 1 summarizes the dimensions of the original design (design-1) used in [1] and the newly developed post designs (design-2 to -4). Design-2 consists of square posts, whose width is reduced to 66% of that of the original design (design-1) with a post width of 6.1 μm. The square posts thus have a width of 4 μm, representing the

Table 1. Dimensions of the post designs used in simulations (sim) and experiments (exp), see also Figs. 1 and 2

Layout	Design-1 (rectangles) (sim and exp)	Design-2 (squares) (sim)	Design-3 (rhomb-like) (sim)	Design-4 (rhomb-like) (sim and exp)
Periodicity (L)	25.6 μm	26 μm	27 μm	27.0 μm
Post size ($b \times a$)	6.1×3.1 μm^2	4×4 μm^2	6×6 μm^2	4.9×3.8 μm^2
Small gap (c)	1.7 μm	1 μm	1 μm	2.2 μm
Large gap (d)	3.1 μm	4 μm	3 μm	5.3 μm
Attraction basin (s)	7.3 μm	4 μm	5 μm	5.1 μm

Posts in all experimental designs were 9 μm high.

smallest width achievable with the lithography methods used here. Design-3 displays rhomb-like shaped posts. The width of these posts (6 μm) is comparable to the width of design-1 (6.1 μm). Design-4 corresponds to the experimentally realized post shape combining both concepts (see Table 1 for dimensions).

3.1 Simulation

In these new designs-2 and -3, we performed simulations with 1.9 μm beads, whose mobility and diffusion have been characterized by Regtmeier *et al.* [19], to check if the expected acceleration of ANM can be observed and to compare the velocities with the previously obtained data from design-1. The results of the simulations together with the previously presented experimental data [1] in design-1 are shown in Fig. 2. Both new geometries demonstrate an increase in velocity (Figs. 2b and c) of more than one order of magnitude compared with design-1 (Fig. 2a). For the square posts (design-2), this is attributed to the reduced dimensions of the basin of attraction which results in a shorter diffusion distance for the particles. Indeed, for the width of the basin of attraction s, we find 4 μm, whereas in the original design-1 s is 7.3 μm (compare Figs. 3a and b, and Table 1). On the other hand, the same enhancement occurs in design-3, where only the shape of the posts was changed retaining the post width. As can be seen from Fig. 3c, the rhomb-like post structure with sharp apexes in design-3 results in $s = 5$ μm, which is ∼32% smaller than in design-1. This means, that not only the post width and the resulting ratio of trap-to-gap width determine the distance s but also the shape of the posts. Despite the different values of s for design-2 and -3, the same enhancement of the ANM velocity is observed. This is attributed to a lower probability of back-diffusion of beads having left the basin of attraction, due to the sharpened apex of the post.

3.2 Experimental acceleration of ANM

Having gained such insight, we experimentally realized an ANM device (design-4) which incorporates both concepts of increasing the velocity as outlined above (see Table 1 for dimensions). The posts have a rhomb-like shape with truncated apexes and a final width of 75% compared with design-1. Due to the limitations of the lithography process, the trap width resulted in 2.2 μm, which was slightly larger than expected. The experiments were thus carried out with 2.9 μm beads. Figure 4a shows the ANM response of about 160 driving periods for each data point. All determined velocities up to $U_{dc} \approx \pm 60$ V demonstrate ANM, *i.e.*, a migration opposite to the static force. The experimental error bars are due to the limited number of beads and observation time. Also shown in Fig. 4a is the simulation curve, for which the actual dimensions of the experimental posts are approximated by the shape as shown in Fig. 3d. The agreement of experiment and simulation is very good as in our previous studies [1, 19]. The comparison of design-1 with design-4 results in an increase in the maximum velocity by a factor of 7. This is remarkable because the diffusion of the 2.9 μm beads is lower by 37% compared with the beads of 1.9 μm used in the measurements of design-1 [1]. It is interesting to note that s in design-3 and -4 results in a similar value (5 and 5.1 μm respectively), although the post width is reduced in design-4. This demonstrates that the width of the basin of attraction also depends on the ratio of the trap-to-gap width.

3.3 Adjustability of migration direction

Aiming at a separation utilizing ANM, the main prerequisite is the availability of two opposite migration directions for different bead species under identical driving conditions. Demonstrating the latter, the separation experiment was performed previously [19], where also the main mechanism responsible for the opposite migration directions of differently sized but alike charged beads was discussed. Here, we focus on the issue of whether transport in the normal direction (*i.e.*, along the dc-bias) is possible with the same bead size and whether it is also accelerated in the new design-4. This was experimentally validated (see Fig. 5) with a velocity enhancement by one order of magnitude compared with the velocities obtained by Regtmeier *et al.* [19].

Migration in the normal direction (*i.e.*, in the direction of the applied force) occurs when the traveled distance,

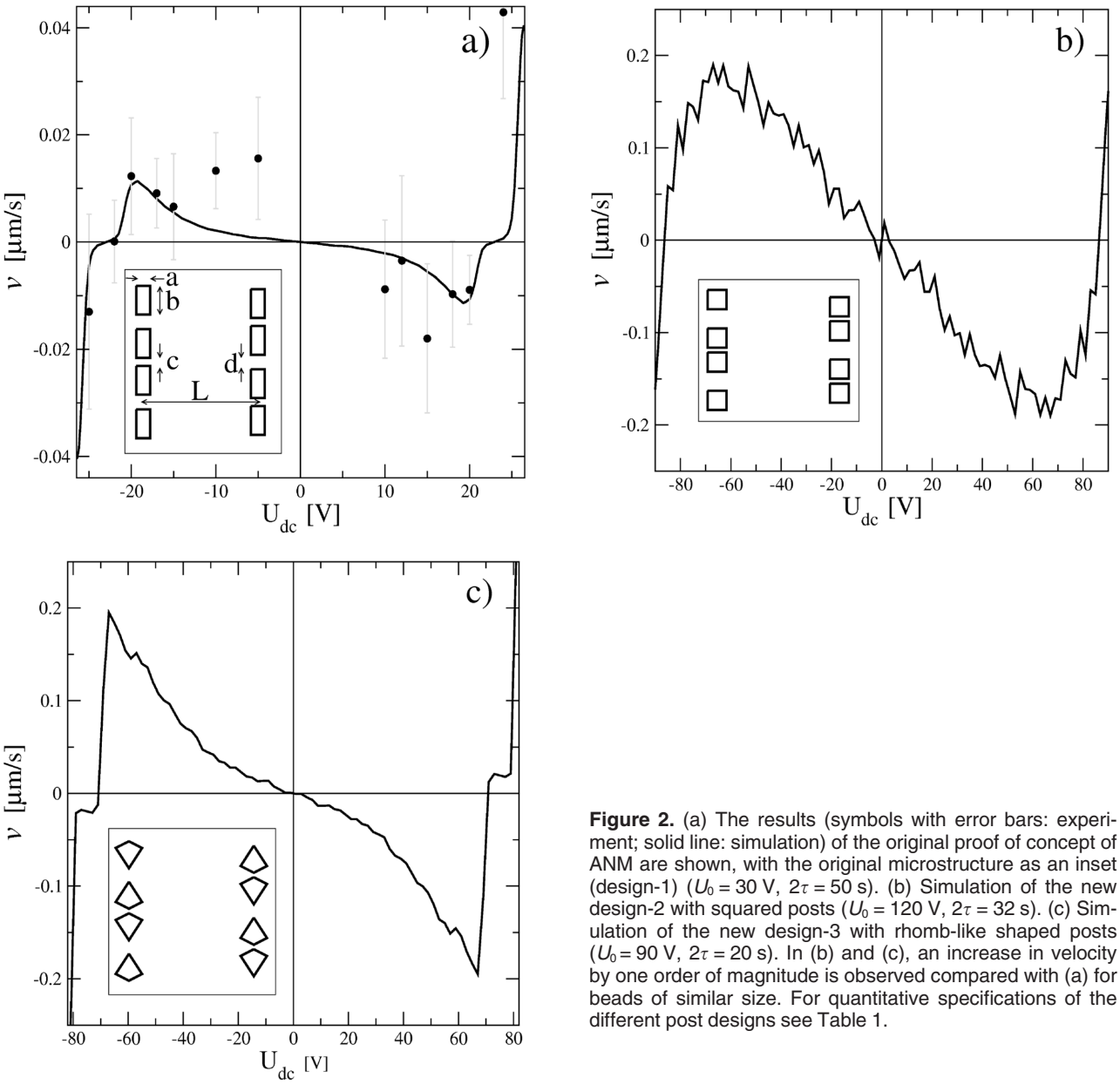

Figure 2. (a) The results (symbols with error bars: experiment; solid line: simulation) of the original proof of concept of ANM are shown, with the original microstructure as an inset (design-1) ($U_0 = 30$ V, $2\tau = 50$ s). (b) Simulation of the new design-2 with squared posts ($U_0 = 120$ V, $2\tau = 32$ s). (c) Simulation of the new design-3 with rhomb-like shaped posts ($U_0 = 90$ V, $2\tau = 20$ s). In (b) and (c), an increase in velocity by one order of magnitude is observed compared with (a) for beads of similar size. For quantitative specifications of the different post designs see Table 1.

during the slow phase, is smaller than the trap-to-trap distance $2L$ (see Fig. 1), as the decision of trap avoiding is made only close to the posts forming the trap. Thus, the particle cannot proceed far enough during the half period τ for avoiding the trap ahead. On the other hand, due to the fact that the bead diffuses during the back and forth motion, it can avoid the trap it started from. Therefore, both directions of migration are possible, depending on the particle properties and driving parameters, and both are enhanced by the optimization of the posts.

4 Concluding remarks

The transport velocities which can be reached for ANM of colloidal particles in a microfluidic device are limited by the diffusion of the particles. With our present study, we demonstrated theoretically and experimentally that the maximum ANM velocities can be enhanced as compared to previous ANM studies [1, 19] by approximately one order of magnitude by optimizing the size and the shape of the posts in the microstructure. This acceleration was achieved despite the fact that larger beads with a lower

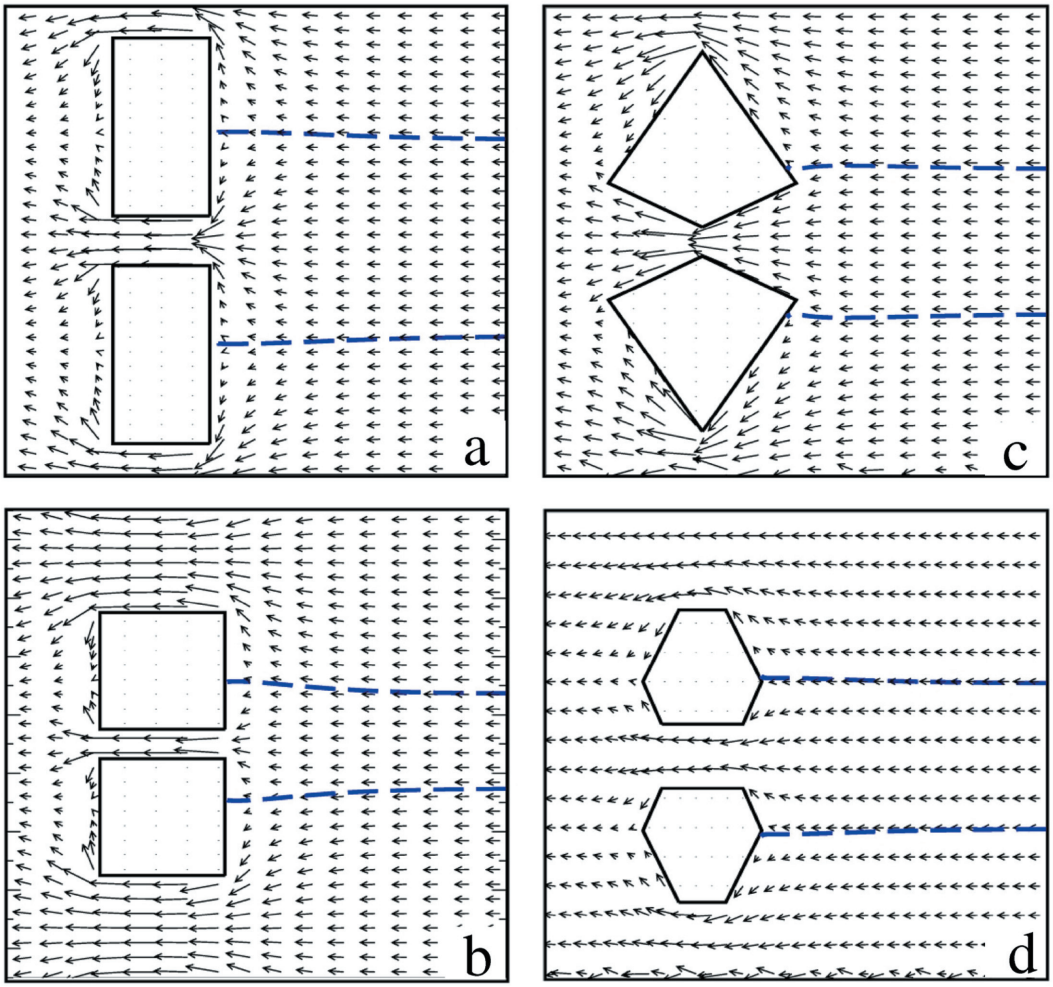

Figure 3. Schematic drawings of geometric traps of design-1, -2, -3, and -4 representing 16 by 16 μm^2. The arrows indicate the strength and direction of the electric field. The dashed lines are the boundaries of the deterministic attraction basin of the small gaps. The width of the basin of attraction can be controlled by the post width, post shape, and the ratio of the widths of the small and large gaps.

diffusion coefficient had to be employed experimentally compared with the beads in ref. [1, 19].

By changing the driving parameters U_0 and τ, it is possible to easily adjust the direction of migration. We demonstrated that also the migration in the normal direction (*i.e.*, along the dc-bias) is accelerated by the same optimizations of the post size and shape that were used for enhancing ANM. With these properties, future separation or fractionation by ANM should demonstrate enhanced transport in opposite directions, thus using both directions of this pulsed field technique advantageously.

Finally, we briefly address the issue of how the ANM velocity scales with the particle size and driving parameters. As already mentioned in Section 1, a decrease in particle size increases the diffusivity and thus enhances the ANM effect. However, this requires a concomitant down-scaling of the post array dimensions, such that the gaps keep their trapping properties for the smaller particles. Moreover, the faster diffusion leads to a larger probability of leaving the attraction basin of the trap also in the fast direction (see Fig. 1), thus diminishing ANM. Hence, the driving parameters have to be adapted as well; in particular, a higher amplitude U_0 has to be chosen. This higher amplitude allows using shorter driving periods, 2τ, leading again to enhanced ANM velocities because the frequency of heading toward a trap is increased and thus the probability *per* time for avoiding a trap. Note, however, that for the occurrence of ANM the particle must be able to travel at least the distance between two traps within the time τ (see Fig. 1) [19] specifying a lower limit for τ.

This discussion shows that the ANM effect depends on all the details of the setup, and that there are no simple

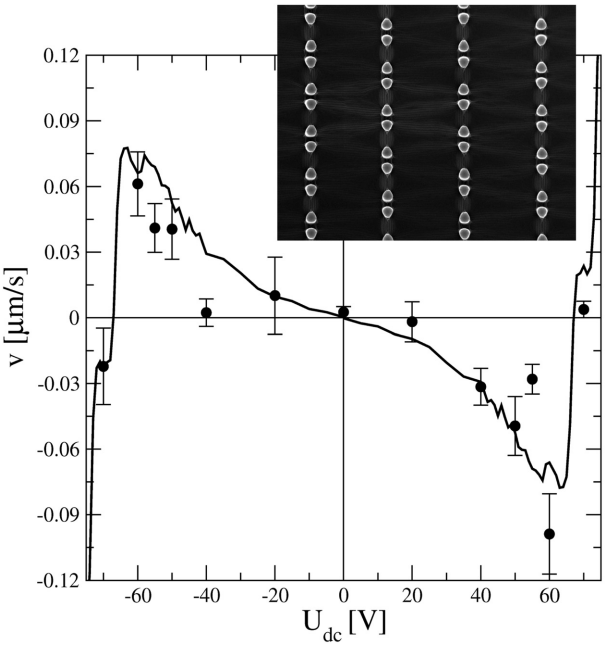

Figure 4. Experimental ANM velocity (dots with error bars) for different U_{dc} in the newly designed post array (design-4) (U_0 = 80 V, 2τ = 60 s). The velocity is increased by about one order of magnitude compared with Fig. 2a, although larger beads (2.9 µm compared with 1.9 µm) had to be used. The black line shows the results obtained from numerical simulations. The fluctuations are due to the limited simulation time. The inset shows an SEM image of the experimentally used design-4 (see Table 1 for dimensions).

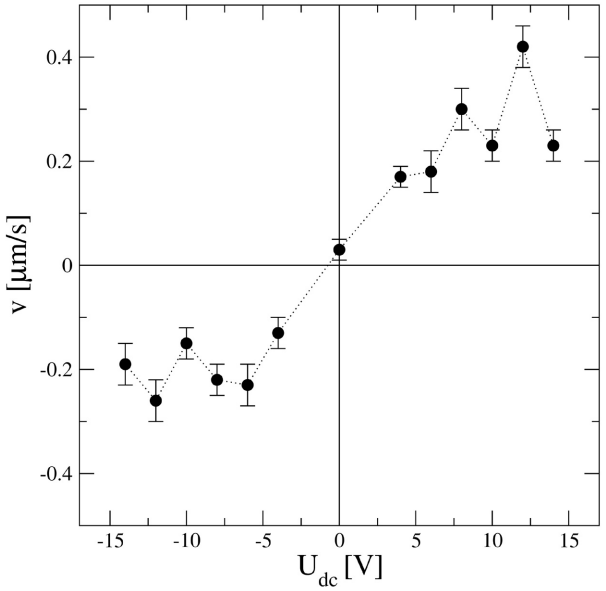

Figure 5. Experimental velocity (dots with error bars) for different U_{dc}s in design-4 (U_0 = 20 V, 2τ = 20 s). Migration in the normal direction (*i.e.*, along the dc-bias) is observed and the velocity is one order of magnitude faster than the velocities obtained by Regtmeier *et al.* [19]. The dashed line is a guide to the eye.

scaling laws for the ANM velocity (see also the theoretical analysis in ref. [13 – 15]). On the other hand, this complex interplay between the system properties is the basis for its flexibility to switch the sign of the average migration velocity by simple adaptation of the driving parameters (*cf.* Figs. 4 and 5), and to guide different particle species into opposite direction under identical driving conditions [19].

Donation of F108 from BASF is gratefully acknowledged. Special thanks is due to Henning Höfemann for assistance with the lithography process. Financial support by the Deutsche Forschungsgemeinschaft within the collaborative research project SFB-613 (project D2) is gratefully acknowledged.

5 References

[1] Ros, A., Eichorn, R., Regtmeier, J., Duong, T. T., Reimann, P., Anselmetti, D., *Nature* 2005, *436*, 928.

[2] Matthias, S., Müller, F., *Nature* 2003, *424*, 53 – 57.

[3] Rousselet, J., Salome, L., Ajdari, A., Prost, J., *Nature* 1994, *370*, 446 – 447.

[4] Faucheux, L. P., Libchaber, A., *Faraday Trans.* 1995, *91*, 3163 – 3166.

[5] Gorre-Talini, L., Spatz, J. P., Silberzan, P., *Chaos* 1998, *8*, 650 – 656.

[6] Marquet, C., Buguin, A., Talini, L., Silberzan, P., *Phys. Rev. Lett.* 2002, *88*, 168301-1-4.

[7] Bader, J., Hammond, R. W., Henck, S. A., Deem, M. W., McDermott, G. A., Bustillo, J. M., Simpson, J. W., Mulhern, G. T., Rothberg, J. M., *PNAS* 1999, *96*, 13165 – 13169.

[8] van Oudenaarden, A., Boxer, S. G., *Science* 1999, *285*, 1046 – 1048.

[9] Huang, L. R., Cox, E. C., Austin, R. H., Sturm, J. C., *Anal. Chem.* 2003, *75*, 6963 – 6967.

[10] Chou, C.-F., Bakajin, O., Turner, W. P., Duke, T., Chan, S. S., Cox, E. C., Craighead, H. G., Austin, R. H., *PNAS* 1999, *96*, 13762 – 13765.

[11] Han, J., Craighead, H. G., *Science* 2000, *288*, 1026 – 1029.

[12] Fu, J., Mao, P., Han, J., *Appl. Phys. Lett.* 2005, *87*, 263902-1-3.

[13] Eichhorn, R., Reimann, P., Hänggi, P., *Phys. Rev. E* 2002, *66*, 066132-1-14.

[14] Eichhorn, R., Reimann, P., Hänggi, P., *Phys. Rev. Lett.* 2002, *88*, 190601-1-4.

[15] Eichhorn, R., Reimann, P., *Acta Phys. Pol., B* 2006, *37*, 1491 – 1501.

[16] Duong, T. T., Kim, G., Ros, R., Streek, M., Schmid, F., Brugger, J., Ros, A., Anselmetti, D., *Microelectron. Eng.* 2003, *67 – 68*, 905 – 912.

[17] Hellmich, W., Regtmeier, J., Duong, T. T., Ros, R., Anselmetti, D., Ros, A., *Langmuir* 2005, *21*, 7551 – 7557.

[18] Huang, L. R., Silberzan, P., Tegenfeldt, J., Cox, E. C., Sturm, J. C., Austin, R. H., Craighead, H., *Phys. Rev. Lett.* 2002, *89*, 178301-1-4.

[19] Regtmeier, J., Duong, T. T., Eichhorn, R., Reimann, P., Anselmetti, D., Ros, A., *Eur. Phys. J. E.* 2007, in press.

